Study of GeSn based heterostructures: towards optimized group IV MQW LEDs

D. Stange,[1,*] N. von den Driesch,[1] D. Rainko,[1] C. Schulte-Braucks,[1] S. Wirths,[1] G. Mussler,[1] A. T. Tiedemann,[1] T. Stoica,[1,2] J. M. Hartmann,[3] Z. Ikonic,[4] S. Mantl,[1] D. Grützmacher,[1] and D. Buca[1]

[1]*Peter Grünberg Institute 9 (PGI 9) and JARA-Fundamentals of Future Information Technologies, Forschungszentrum Juelich, 52425 Juelich, Germany*
[2]*National Institute of Materials Physics, P.O. Box MG-7, Magurele, Bucharest 077125, Romania*
[3]*Univ. Grenoble Alpes, F-38000 and CEA, LETI, MINATEC Campus, F-38054 Grenoble, France*
[4]*Institute of Microwaves and Photonics, School of Electronic and Electrical Engineering, University of Leeds, Leeds LS2 9JT, UK*
[*]*d.stange@fz-juelich.de*

Abstract: We present results on CVD growth and electro-optical characterization of $Ge_{0.92}Sn_{0.08}$/Ge *p-i-n* heterostructure diodes. The suitability of Ge as barriers for direct bandgap GeSn active layers in different LED geometries, such as double heterostructures and multi quantum wells is discussed based on electroluminescence data. Theoretical calculations by effective mass and 6 band k·p method reveal low barrier heights for this specific structure. Best configurations offer only a maximum barrier height for electrons of about 40 meV at the Γ point at room temperature (e.g. 300 K), evidently insufficient for proper light emitting devices. An alternative solution using SiGeSn as barrier material is introduced, which provides appropriate band alignment for both electrons and holes resulting in efficient confinement in direct bandgap GeSn wells. Finally, epitaxial growth of such a complete SiGeSn/GeSn/SiGeSn double heterostructure including doping is shown.

OCIS codes: (230.0250) Optoelectronics; (230.3670) Light-emitting diodes.

References and links

1. S. Wirths, R. Geiger, N. von den Driesch, G. Mussler, T. Stoica, S. Mantl, Z. Ikonic, M. Luysberg, S. Chiussi, J. M. Hartmann, H. Sigg, J. Faist, D. Buca, and D. Grützmacher, "Lasing in direct-bandgap GeSn alloy grown on Si," Nat. Photonics **9**(2), 88–92 (2015).
2. D. Stange, S. Wirths, N. von den Driesch, G. Mussler, T. Stoica, Z. Ikonic, J. M. Hartmann, S. Mantl, D. Grützmacher, and D. Buca, "Optical transitions in direct-bandgap Ge1– x Snx alloys," ACS Photonics **2**(11), 1539–1545 (2015).
3. Z. Alferov, "Double heterostructure lasers: Early days and future perspectives," IEEE J. Sel. Top. Quantum Electron. **6**(6), 832–840 (2000).
4. J. D. Gallagher, C. L. Senaratne, P. Sims, T. Aoki, J. Menéndez, and J. Kouvetakis, "Electroluminescence from GeSn heterostructure pin diodes at the indirect to direct transition," Appl. Phys. Lett. **106**(9), 091103 (2015).
5. M. Oehme, K. Kostecki, T. Arguirov, G. Mussler, K. Ye, M. Gollhofer, M. Schmid, M. Kaschel, R. A. Korner, M. Kittler, D. Buca, E. Kasper, and J. Schulze, "GeSn heterojunction LEDs on Si substrates," IEEE Photonics Technol. Lett. **26**(2), 187–189 (2014).
6. H. H. Tseng, K. Y. Wu, H. Li, V. Mashanov, H. H. Cheng, G. Sun, and R. Soref, "Mid-infrared electroluminescence from a Ge/Ge0.922Sn0.078/Ge double heterostructure p-i-n diode on a Si substrate," Appl. Phys. Lett. **102**(18), 182106 (2013).
7. W. Du, Y. Zhou, S. A. Ghetmiri, A. Mosleh, B. R. Conley, A. Nazzal, R. A. Soref, G. Sun, J. Tolle, J. Margetis, H. A. Naseem, and S.-Q. Yu, "Room-temperature electroluminescence from Ge/Ge1-xSnx/Ge diodes on Si substrates," Appl. Phys. Lett. **104**(24), 241110 (2014).
8. J. P. Gupta, N. Bhargava, S. Kim, T. Adam, and J. Kolodzey, "Infrared electroluminescence from GeSn heterojunction diodes grown by molecular beam epitaxy," Appl. Phys. Lett. **102**(25), 251117 (2013).
9. B. Schwartz, M. Oehme, K. Kostecki, D. Widmann, M. Gollhofer, R. Koerner, S. Bechler, I. A. Fischer, T. Wendav, E. Kasper, J. Schulze, and M. Kittler, "Electroluminescence of GeSn/Ge MQW LEDs on Si substrate," Opt. Lett. **40**(13), 3209–3212 (2015).

#254548 Received 24 Nov 2015; revised 29 Dec 2015; accepted 30 Dec 2015; published 15 Jan 2016

10. I. A. Fischer, T. Wendav, L. Augel, S. Jitpakdeebodin, F. Oliveira, A. Benedetti, S. Stefanov, S. Chiussi, G. Capellini, K. Busch, and J. Schulze, "Growth and characterization of SiGeSn quantum well photodiodes," Opt. Express **23**(19), 25048–25057 (2015).
11. A. Gassenq, F. Gencarelli, J. Van Campenhout, Y. Shimura, R. Loo, G. Narcy, B. Vincent, and G. Roelkens, "GeSn/Ge heterostructure short-wave infrared photodetectors on silicon," Opt. Express **20**(25), 27297–27303 (2012).
12. M. Oehme, D. Widmann, K. Kostecki, P. Zaumseil, B. Schwartz, M. Gollhofer, R. Koerner, S. Bechler, M. Kittler, E. Kasper, and J. Schulze, "GeSn/Ge multiquantum well photodetectors on Si substrates," Opt. Lett. **39**(16), 4711–4714 (2014).
13. Y.-H. Kuo, Y. K. Lee, Y. Ge, S. Ren, J. E. Roth, T. I. Kamins, D. A. B. Miller, and J. S. Harris, "Strong quantum-confined Stark effect in germanium quantum-well structures on silicon," Nature **437**(7063), 1334–1336 (2005).
14. R. A. Soref, G. Sun, and H. H. Cheng, "Franz-Keldysh electro-absorption modulation in germanium-tin alloys," J. Appl. Phys. **111**(12), 123113 (2012).
15. C. Schulte-Braucks, D. Stange, N. von den Driesch, S. Blaeser, Z. Ikonic, J. M. Hartmann, S. Mantl, and D. Buca, "Negative differential resistance in direct bandgap GeSn p-i-n structures," Appl. Phys. Lett. **107**(4), 042101 (2015).
16. J. M. Hartmann, A. Abbadie, N. Cherkashin, H. Grampeix, and L. Clavelier, "Epitaxial growth of Ge thick layers on nominal and 6° off Si(001); Ge surface passivation by Si," Semicond. Sci. Technol. **24**(5), 055002 (2009).
17. N. von den Driesch, D. Stange, S. Wirths, G. Mussler, B. Holländer, Z. Ikonic, J. M. Hartmann, T. Stoica, S. Mantl, D. Grützmacher, and D. Buca, "Direct bandgap group IV epitaxy on Si for laser applications," Chem. Mater. **27**(13), 4693–4702 (2015).
18. S. Wirths, D. Buca, G. Mussler, A. T. Tiedemann, B. Holländer, P. Bernardy, T. Stoica, D. Grützmacher, and S. Mantl, "Reduced pressure CVD growth of Ge and Ge1-xSnx alloys," ECS J. Solid State Sci. Technol. **2**(99–N), 102 (2013).
19. F. Gencarelli, B. Vincent, J. Demeulemeester, A. Vantomme, A. Moussa, A. Franquet, A. Kumar, H. Bender, J. Meersschaut, W. Vandervorst, R. Loo, M. Caymax, K. Temst, and M. Heyns, "Crystalline Properties and Strain Relaxation Mechanism of CVD Grown GeSn," ECS J. Solid State Sci. Technol. **2**(4), P134–P137 (2013).
20. S. Wirths, R. Troitsch, G. Mussler, J.-M. Hartmann, P. Zaumseil, T. Schroeder, S. Mantl, and D. Buca, "Ternary and quaternary Ni(Si)Ge(Sn) contact formation for highly strained Ge p- and n-MOSFETs," Semicond. Sci. Technol. **30**(5), 055003 (2015).
21. J. Menéndez and J. Kouvetakis, "Type-I Ge/$Ge_{1-x-y}Si_xSn_y$ strained-layer heterostructures with a direct Ge bandgap," Appl. Phys. Lett. **85**(7), 1175 (2004).
22. M. Jaros, "Simple analytic model for heterojunction band offsets," Phys. Rev. B Condens. Matter **37**(12), 7112–7114 (1988).
23. S. L. Chuang, *Physics of Optoelectronic Devices* (Wiley, 1995).
24. K. Lu Low, Y. Yang, G. Han, W. Fan, and Y.-C. Yeo, "Electronic band structure and effective mass parameters of Ge1−xSnx alloys," J. Appl. Phys. **112**(10), 103715 (2012).
25. V. R. D'Costa, Y. Y. Fang, J. Tolle, J. Kouvetakis, and J. Menéndez, "Tunable optical gap at a fixed lattice constant in group-IV semiconductor alloys," Phys. Rev. Lett. **102**(10), 107403 (2009).
26. S. Wirths, D. Buca, Z. Ikonic, P. Harrison, A. T. Tiedemann, B. Holländer, T. Stoica, G. Mussler, U. Breuer, J. M. Hartmann, D. Grützmacher, and S. Mantl, "SiGeSn growth studies using reduced pressure chemical vapor deposition towards optoelectronic applications," Thin Solid Films **557**, 183–187 (2014).
27. G. Sun, R. A. Soref, and H. H. Cheng, "Design of a Si-based lattice-matched room-temperature GeSn/GeSiSn multi-quantum-well mid-infrared laser diode," Opt. Express **18**(19), 19957–19965 (2010).
28. G. Chang, S. Chang, and S. L. Chuang, "Strain-Balanced GezSn1-z/SixGeySn1-x-y Multiple-Quantum-Well Lasers," IEEE J. Quantum Electron. **46**(12), 1813–1820 (2010).
29. M. Bauer, C. Ritter, P. Crozier, J. Ren, J. Menendez, G. Wolf, and J. Kouvetakis, "Synthesis of ternary SiGeSn semiconductors on Si(100) via Sn_xGe_{1-x} buffer layers," Appl. Phys. Lett. **83**(11), 2163 (2003).
30. C. L. Senaratne, J. D. Gallagher, T. Aoki, J. Kouvetakis, and J. Menéndez, "Advances in light emission from group-IV alloys via lattice engineering and n-type doping based on custom-designed chemistries," Chem. Mater. **26**(20), 6033–6041 (2014).
31. M. Y. Ryu, T. R. Harris, Y. K. Yeo, R. T. Beeler, and J. Kouvetakis, "Temperature-dependent photoluminescence of Ge/Si and Ge $_{1-y}Sn_y$/Si, indicating possible indirect-to-direct bandgap transition at lower Sn content," Appl. Phys. Lett. **102**(17), 171908 (2013).
32. P. Moontragoon, R. A. Soref, and Z. Ikonic, "The direct and indirect bandgaps of unstrained SixGe1−x−ySny and their photonic device applications," J. Appl. Phys. **112**(7), 073106 (2012).

1. Introduction

Group-IV light sources based on direct bandgap GeSn and indirect bandgap SiGeSn alloys, which can be monolithically integrated on silicon, receive rising attention currently. Indeed, the incorporation of Sn in the Ge crystal reduces the conduction band energy of Γ-valley

#254548 Received 24 Nov 2015; revised 29 Dec 2015; accepted 30 Dec 2015; published 15 Jan 2016

faster than the L-valley, resulting in a transition from indirect to direct bandgap semiconductor. This occurs at a Sn concentration of around 9 at. % for a cubic lattice structure [1] and depends sensitively on the residual compressive strain in tetragonal crystal structures [2]. The experimental proof of this transition has led to the first demonstration of optically pumped direct bandgap GeSn lasers in early 2015 [1]. This fundamental breakthrough increased the hope and the efforts for the realization of an efficient electrically pumped Si based light source for optoelectronic on-chip applications.

The winning ways of III-V lasers can be taken as guidance for the development of GeSn light sources: the injection current threshold for lasing was dramatically reduced by the use of carrier confining heterostructures, such as double heterostructures (DHS) or multi quantum wells (MQWs) [3]. The charge carriers in those structures are spatially confined to the optically active region, leading to enhanced radiative recombination rates. Along these lines, the lasing threshold current density could be reduced by several orders of magnitude compared to homojunction structures, due to the dimensionality induced changes of the density of states. GeSn based heterostructures are thus most promising for the fabrication of electrically pumped group IV lasers and efficient light emitting diodes.

Light emitting diodes (LED) fabricated from *p-i-n* GeSn homojunction structures have already been reported [4] and confirmed the expectation of enhanced light emission compared to Ge LEDs [5]. Different approaches in order to integrate GeSn active layers in LEDs have been explored in recent years, ranging from Ge/GeSn/Ge DHS [5–8] to more advanced structures as {Ge/GeSn} [9] and {Ge/SiGeSn} MQWs [10]. More detailed LED characteristics were investigated in [9]. The studies involved highly compressively strained GeSn layers, which maintain their indirectness and require large injection currents [5]. The realization of high epitaxial quality MQW heterostructures and control of doping leads to versatile semiconductor stacks important not only for LEDs. They also offer advantages for light detectors [11,12] or optical modulators based on the quantum confined Stark effect, where strong spectral shift of the absorption edge with an applied electric field can be induced [13,14]. Moreover, such heterostructures can improve tunneling effects, like negative differential resistance in tunneling diodes, recently demonstrated in [15] for *p-i-n* $Ge_{0.89}Sn_{0.11}$ homojunctions.

In this work we present the epitaxial growth and structural as well as electro-optical characterization of *p-i-n* $Ge_{0.915}Sn_{0.085}$/Ge DHS and MQW LEDs. We discuss, based on theoretical calculations, the limitations of Ge as barriers for both configurations employing GeSn wells with Sn contents between 0 - 15 at. %. We show that Ge layers are ineffective barriers for direct bandgap GeSn wells. Instead, we demonstrate that MQW heterostructures with direct bandgap GeSn wells, type I alignment for both L and Γ- valleys and reasonable barrier-well offsets can be obtained in {SiGeSn/GeSn} MQWs.

2. Epitaxial growth and material characterization

The GeSn based heterostructures were grown on top of 2.5 µm thick Ge virtual substrate (Ge-VS) on Si(100) [16] by reactive gas source epitaxy (RGSE). Digermane (Ge_2H_6) and Tin tetrachloride ($SnCl_4$) are used as precursor gases, which are introduced into the reaction chamber with a showerhead for homogeneous gas distribution for 200 mm wafers [17,18]. To allow efficient carrier injection and avoid ion implantation induced damage, the layers were in situ n-type and p-type doped employing phosphine (PH_3) and diborane (B_2H_6), respectively. The complete {Ge/GeSn} MQW structure was grown at 375°C. All Sn concentrations are determined by Rutherford Backscattering Spectrometry (RBS). Details can be found in [17]. The bottom layer of the LED structure is a 115 nm thick, partially strain relaxed $Ge_{0.92}Sn_{0.08}$:B layer. It serves as hole injection layer with an active carrier concentration of about $4x10^{18}$ cm^{-3}, as determined by electrochemical capacitance-voltage profiling (ECV). This approach is beneficial compared to the use of in situ doped bulk Ge, as it allows a partial relaxation of the GeSn layers with a misfit dislocation network confined at

#254548 Received 24 Nov 2015; revised 29 Dec 2015; accepted 30 Dec 2015; published 15 Jan 2016

the GeSn/Ge interface below the optically active device layer stack. The epitaxial growth continues with the deposition of a 20 nm thick tensely strained Ge layer, followed by the MQW active region consisting of seven 20 nm thick $Ge_{0.92}Sn_{0.08}$ quantum wells separated by 14 nm thick Ge barrier layers. The MQW stack is finalized by a 20 nm thick Ge barrier layer and capped by a 60 nm thick phosphorous doped $Ge_{0.92}Sn_{0.08}$ film with a doping concentration of $7.5x10^{19}$ cm^{-3}. The latter acts as electron injection layer, completing the LED heterostructure. For the purposes of comparison, a second set of samples was grown under the same conditions, comprising a *p-i-n* $Ge_{0.92}Sn_{0.08}$ homojunction.

The cross-sectional transmission electron micrograph (XTEM) presented in Fig. 1(a) reveals a high crystalline quality with smooth interfaces between GeSn wells and Ge barriers, as shown in the inset. The chemical abruptness of the interfaces between GeSn and Ge is revealed by the secondary ion mass spectroscopy (SIMS) depth profile of Sn, shown as an overlay in Fig. 1(a). Additionally, phosphorous and boron atoms in the electron and hole injection layers could be resolved by SIMS, with rather sharp elementary boundaries.

Residual strain of individual layers in the structure can be quantified by X-ray diffraction reciprocal space mapping (XRD-RSM) around the asymmetric (224) reflection as depicted in Fig. 1(b). The required elastic constants for the GeSn allys are taken from [19]. The GeSn:B buffer contains a residual compressive strain of roughly –0.71%, inducing a 0.48% tensile strain in the Ge barriers pseudomorphically grown on top. The Ge/GeSn MQW has the same in-plane lattice parameter like the partially relaxed GeSn:B layer without introduction of crystal defects, as indicated by the dashed line in Fig. 1(b). Additionally, distinct satellite peaks can be seen from a 2θ-θ scan (carried out around the (004) reflection) of the growth structure in Fig. 1(c). The simulation yields sample parameters (thickness of GeSn well and Ge barrier, Sn content of the well) in agreement with the nominal values.

The comparison *p-i-n* $Ge_{0.92}Sn_{0.08}$ homojunction has a total thickness of the GeSn structure of around 500 nm, including an active region of about 350 nm, which allows for a larger degree of relaxation, with a residual compressive strain of –0.21% only.

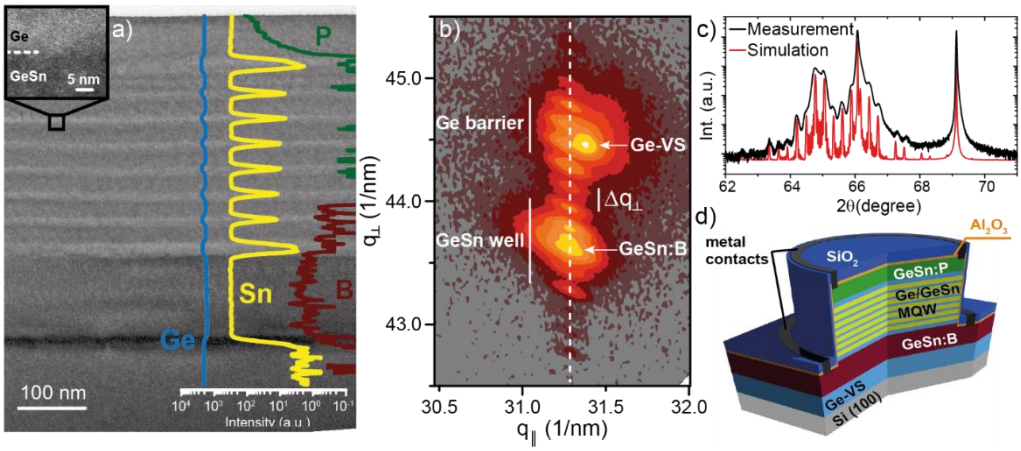

Fig. 1. (a) XTEM micrograph of the MQW heterostructure shows high crystalline quality and abrupt interfaces (inset). An overlaid SIMS profile confirms the layer morphology. (b) Residual strain of the GeSn well (–0.71%) and Ge barrier (0.48%) can be extracted from XRD-RSM. (c) Satellite peaks in 2θ-θ scan match well the simulation. (d) Schematic profile of the fabricated light emitting diode.

3. Device fabrication and characterization

Fabrication of LEDs was performed by only employing standard Si process technology. First, the device mesas were etched by Cl_2/Ar reactive ion etching (RIE). Mesa passivation was performed by a two layer stack containing 10 nm Al_2O_3 deposited by atomic layer deposition

#254548 Received 24 Nov 2015; revised 29 Dec 2015; accepted 30 Dec 2015; published 15 Jan 2016

(ALD) at 300°C and 150 nm SiO_2 deposited by plasma enhanced chemical vapor deposition (PECVD) at 300°C. Optical lithography and Al_2O_3/SiO_2 RIE was applied to open contact windows with CHF_3 plasma. Low resistance metallic NiGeSn is formed by sputtering of 10 nm Ni and forming gas annealing (N_2:H_2 / 4:1) at 325°C [20] followed by Al deposition as an additional contact layer. A schematic profile of the fabricated device is shown in Fig. 1(c).

Electroluminescence (EL) measurements were performed in a liquid He cooled cryostat between 4 K and 300 K, with a 1988 Hz pulsed voltage excitation. The temperature dependent EL spectra, attributed to the Γ- valley emission, are shown in Fig. 2(a) for a 100 µm diameter MQW diode at a current density of 420 A/cm^2. The EL peak at room temperature is at 0.59 eV. The room temperature (RT) spectrum features oscillations, whose spacings are associated to Fabry-Perot modes between Ge-VS/Si and GeSn/air interfaces. With decreasing temperature the blue shift of the EL emission peak occurs (E_{max}(4 K) = 0.61 eV), as expected from the temperature dependence of the bandgap. The integrated EL intensity features a slight *decrease* between 300 K and 100 K followed by a strong *increase* below 100 K, inset of Fig. 2(a). This behavior is related to the indirect bandgap of the GeSn QWs, with a Γ to L-valley separation of about $\Delta E_{\Gamma L}$ = –50 meV, as calculated by k·p and deformation potential model with strain, e.g [21]. (using parameters listed in [1] SI, and averaged valence band offset from [22]). This peculiar evolution of the EL integrated intensity with temperature is caused by an interplay of thermally activated carrier transfer from L- to Γ-valley, and the temperature dependence of recombination velocities of carriers in the L- and Γ-valley. With decreasing temperature the relative number of carriers gaining enough energy to overcome the potential hill between L- and Γ-valley decreases, leading to a decrease in intensity of the EL in the regime from 300 K to 200 K. Below 200 K the pronounced decrease in non-radiative recombination velocity leads to band filling of the L-valley overcompensating the reduced thermal activation and thus causing a strong increase in light emission. The dependence of the EL emission on the injection current density for the MQW is shown in Fig. 2(c), together with that of a *p-i-n* $Ge_{0.92}Sn_{0.08}$ homojunction LED for comparison in Fig. 2(b). The injection current densities necessary to obtain clearly visible spectra are similar for both LEDs, with values ranging from 35 A/cm^2 to 50 A/cm^2, comparable to those reported in [7]. Compared to the homojunction LED, the blue shift of about 14 meV for the MQW EL peak position is mainly associated to the elevated residual compressive strain of –0.71%, since the theoretical expected energy shift for n = 1 (n = 1(HH)) is 5.75 meV (2.96 meV). Despite the strong EL emission from both devices, no beneficial impact of quantum confinement in the MQW geometry on emission threshold current (necessary to produce a clear EL signal) could be observed.

In order to gain a deeper understanding of the MQW emission spectra, the electronic band structure was calculated using the effective mass method for the conduction band and 6-band k·p model for the valence band. Electronic band alignment in the active region of the MQW sample is shown in Fig. 2(d). The theoretical calculations clearly indicate that the GeSn quantum wells are fundamental indirect bandgap semiconductors. Moreover, the structure lacks type I alignment in the conduction band. The heterostructure provides confinement for Γ- electrons, with a barrier height of ΔE_Γ = 29 meV. For the L-valley electrons, the GeSn layers play the role of barriers, with ΔE_L = 18 meV, and the carriers are confined in the strained Ge layers, thus the transition is indirect in k- and in real space. However, for both, Γ- and L-valley electrons, the energy offsets are near the thermal energy at room temperature (k_BT ~25 meV). The holes are confined in the GeSn in heavy hole (HH) states with a barrier height of ΔE_{HH} = 81 meV. Light hole (LH) states are found are energetically less favorable and the barrier is only ΔE_{LH} = 28 meV. The calculated band alignment indicates that the interplay between compressive strain in the GeSn well and the tensile strain in the Ge barrier does not offer sufficient carrier confinement. The resulting LED device is thus not efficient.

#254548 Received 24 Nov 2015; revised 29 Dec 2015; accepted 30 Dec 2015; published 15 Jan 2016

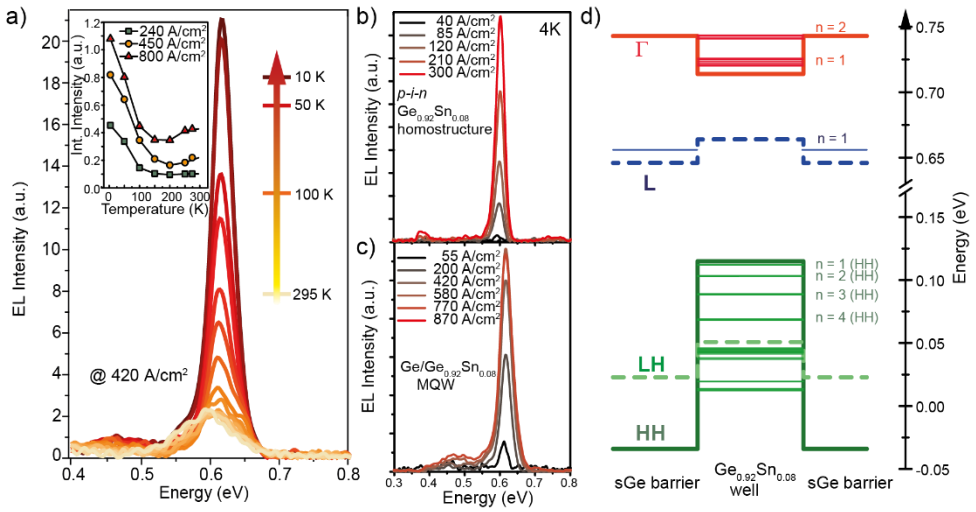

Fig. 2. (a) Temperature dependent EL spectra for a current density of 420 A/cm^2. The inset shows integrated intensities for different injection current densities. (b,c) Injection current dependent El spectra for (b) *p-i-n* GeSn homojunction and (c) GeSn/Ge MQW LEDs of 100 µm diameter. (d) The calculated electronic structure at RT for GeSn/Ge MQW with –0.71% strain in GeSn (+ 0.48% in Ge) showing no confinement of electrons.

To optimize MQW LEDs for low current injection density thresholds and high emission efficiency, the most important requirement is to create a direct bandgap GeSn well with type I band alignment and suitable barrier heights ($\Delta E > k_B T$). In the next section an analysis of optimal configurations fulfilling these conditions is demonstrated.

4. Band structure calculations for MQW configurations

The electronic band structure calculations for MQWs were made using the effective mass approximation for electrons in the conduction bands and 6-band k·p model for holes in the valence band [23]. To develop a general concept, we first address the band alignment in Ge/GeSn DHS as it depends on the Sn content and strain conditions. An optimized structure should have type I band alignment with pronounced band offsets for electrons and holes as well as a fundamental direct bandgap of the GeSn layer. The structure features a fully strain relaxed $Ge_{1-x}Sn_x$ buffer, which defines the actual strain in the pseudomorphically grown $\{Ge/Ge_{1-y}Sn_y\}$ heterostructure on top of it. The Sn content in $Ge_{1-x}Sn_x$ buffer is varied in the epitaxially achievable range of 0-15 at. %. This leads to a wide span of strain values in $Ge_{1-y}Sn_y$ layers: from –2.35% compressive strain for $Ge_{0.85}Sn_{0.15}$ on a relaxed Ge buffer and up to + 2.23% tensile strain for Ge on a relaxed $Ge_{0.85}Sn_{0.15}$ buffer. The regions in which the well material is a fundamental direct bandgap semiconductor is defined by strain and Sn content. The direct/indirect regions depend on the Sn content in buffer and well, as shown in Fig. 3(a). For small Sn concentrations both buffer and well have an indirect band gap (part I). In the remaining region, the GeSn well is a fundamental direct bandgap semiconductor. We can then further restrict the LED structure parameters by adding yet another requirement: type I alignment between barriers and wells, in order to have a large matrix element for radiative electron hole recombination. The remaining interesting region for LEDs is now restricted to part III in Fig. 3(a). Moreover, at a Sn content of 11 at. % in the buffer, the strain in the Ge barrier is sufficiently large to convert Ge into a direct bandgap semiconductor (right of the dashed line). In this region the bandgap of tensile strained Ge is close to, and at higher strains even lower than that of GeSn, as shown in Fig. 3(b). Therefore, in the area on the right of the dashed line in part III the band offsets are small, leading to a reduced confinement of carriers in the GeSn well, leaving only a small region of interest, on the left of the dashed line in part

#254548 Received 24 Nov 2015; revised 29 Dec 2015; accepted 30 Dec 2015; published 15 Jan 2016

III in Fig. 3(a), for GeSn LEDs fabrication. Nevertheless, the region of direct gap Ge could be interesting for Ge based LEDs.

A high degree of carrier confinement inside the well is required when aiming at room temperature light emitting devices. The band offsets should therefore be higher than 25 meV (k_BT at 300 K) while the lowest occupied state should be Γ-type in character. The calculated barrier heights for electrons in Γ- and L- valleys, coming from the combined effects of material composition and strain, are presented in Fig. 3(c), where the blue region indicates highest barrier values. The L barrier increases with increasing Sn content in the well, and is almost independent of Sn content in the substrate (and in fact the "well" layer is the barrier for L-electrons, as discussed above). The confinement of Γ electrons increases for higher values of Sn content in the well and lower Sn contents in the buffer underneath. However, throughout the practically accessible range of parameters considered here (alloy compositions and values of strain), the barrier heights for Γ (max. 40 meV) and L (max. 41.4 meV) bands hardly exceed $1.5 \cdot k_BT$ at 300 K. Hence the GeSn well will not confine electrons effectively, even in cases when the conduction band minimum appears at the Γ–valley, and even if quantization effects are negligible.

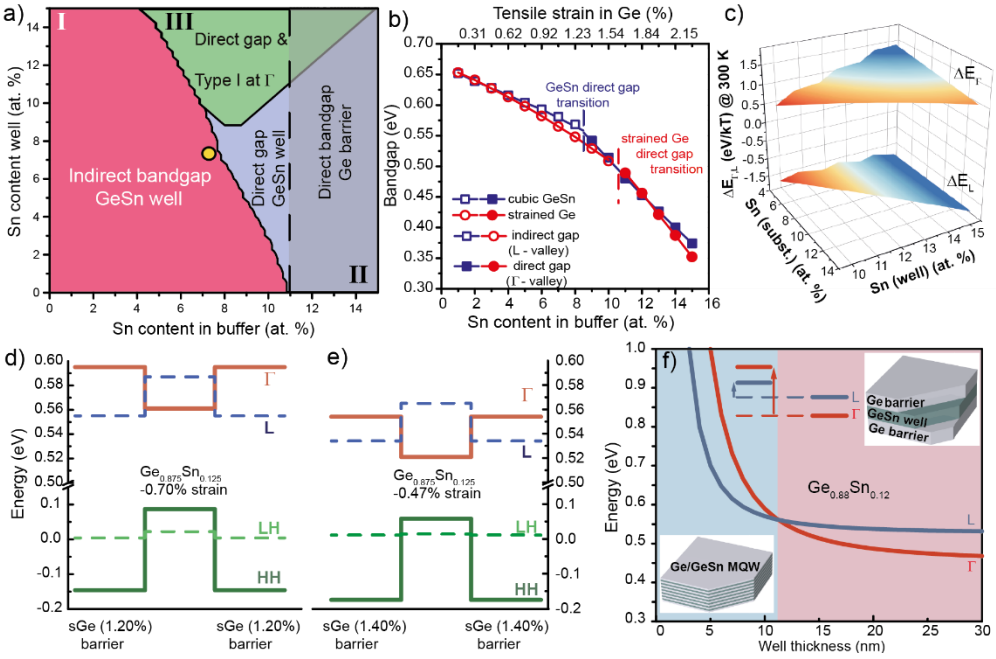

Fig. 3. (a) Regions of the GeSn/Ge QW parameter space (the in-plane lattice constant being determined by the fully relaxed GeSn buffer composition, and Sn concentration in the well) delivering different structure behaviors. The yellow dot represents the position of the experimentally investigated {sGe/$Ge_{0.92}Sn_{0.08}$} MQW (neglecting quantization effects). The deviation of the dot position (7 at. % well Sn concentration vs. 8 at. % inside the grown structure) results from the residual strain inside the device structure because of a non-fully relaxed buffer underneath. (b) Bandgap evolution of GeSn and strained Ge in in-plane lattice matched Ge/GeSn heterostructures. (c) Barrier heights at L and Γ in a Ge/GeSn/Ge structure depending on Sn contents in the GeSn buffer and the well. (d), (e) Band structure of direct bandgap Ge/ $Ge_{0.88}Sn_{0.12}$ /Ge with different compressive strain values. (f) Effect of the well thickness on $Ge_{0.88}Sn_{0.12}$ bandgap: the quantization may change the semiconductor bandgap from direct into indirect (if the lowest Γ-quantized state comes above L, as the well becomes thinner).

After this general discussion of cubic GeSn DHS, let us consider cases of experimentally achievable Ge/GeSn DHS, where the GeSn is a direct bandgap semiconductor, including residual compressive strain. In Figs. 3(d) and 3(e) we present the energy band calculations for

#254548 Received 24 Nov 2015; revised 29 Dec 2015; accepted 30 Dec 2015; published 15 Jan 2016

such a heterostructure harboring a $Ge_{0.875}Sn_{0.125}$ well with either –0.70% or –0.47% compressive strain, respectively. Details on growth of strain relaxed $Ge_{0.875}Sn_{0.125}$ and photoluminescence characterization can be found in [2]. At a compressive strain of –0.71%, $Ge_{0.875}Sn_{0.125}$ is a direct bandgap semiconductor with type II alignment in the DHS. Here, the conduction band minimum at the Γ point is only slightly above the conduction band minimum in the L-valley of the Ge barrier. Decreasing the compressive strain to –0.47%, as shown in Fig. 3(e), results in a reduced bandgap of the GeSn layer and type I heterostructure. Still, the Γ-valley in GeSn is only 13 meV below the L-valley in the 1.4% strained Ge barrier.

Clearly, the GeSn/Ge DHS system has only a very limited applicable and a desired strong carrier confinement is missing. When moving further towards quantum well structures, quantization effects will further reduce the carrier confinement. Moreover, due to the smaller effective mass of Γ-electrons compared to L-electrons [24], quantization will increase the bandgap at Γ faster than at L, shrinking the region where the structure remains effectively a direct bandgap semiconductor, see Fig. 3(f). Consequently the use of Ge/GeSn multilayers as efficient MQW LEDs is questionable: most of the electrons therein will reside in the L- valley of the Ge barriers.

Using indirect bandgap SiGeSn ternaries as barrier materials solves this problem. SiGeSn alloys indeed offer the possibility of tuning the bandgap and strain separately [25,26] and have been proposed as useful materials for group IV laser applications earlier [27,28]. Epitaxial growth of single layers or heterostructures with a large range of Sn compositions (up to 15 at. %) and Si contents (up to 20 at. %) has been reported [10,29,30]. Such SiGeSn alloys possess an indirect bandgap of up to 0.95 eV, much larger than the 0.5 eV for the direct gap $Ge_{0.875}Sn_{0.125}$ binary, used recently for GeSn laser demonstration [1]. Furthermore, incorporation of Si in GeSn reduces the lattice constant which even induces tensile strain in SiGeSn layers grown on GeSn. However, the CVD epitaxial growth conditions, i.e. temperature and precursor flow rates, reduce in practice the range of SiGeSn stoichiometry available [26]. At low growth temperatures e.g. below 350°C, required for the growth of GeSn alloys with Sn > 12 at. %, the incorporation of high Si contents is challenging. The latter is a direct consequence of the higher chemical stability of Si_2H_6 compared to Ge_2H_6 leading to small number of reactive SiH_x radicals on the surface at low temperatures. However, in order to create an efficient barrier layer for GeSn wells, large Si contents are desirable.

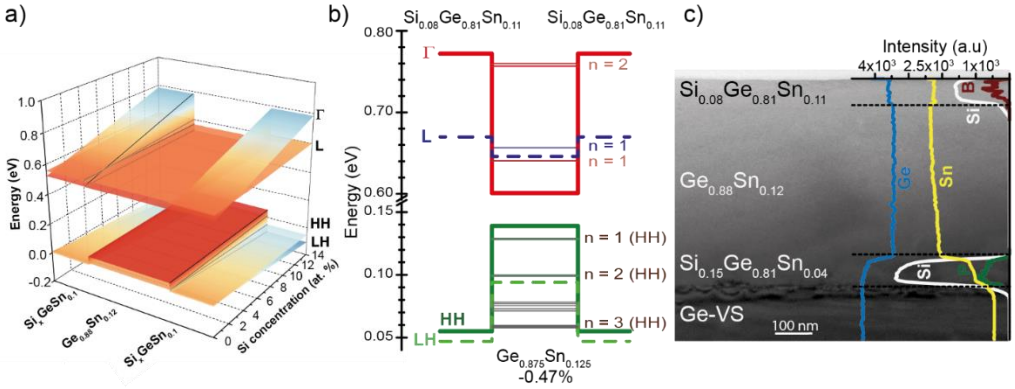

Fig. 4. (a) Calculated energy band alignment for SiGeSn/GeSn heterostructure as a function of the Si content in the SiGeSn cladding layer. (b) Theoretical band alignment, and electron/hole quantized states (minibands) in a 20 nm /10 nm {SiGeSn/GeSn} MQW structure and (c) SIMS and TEM of a SiGeSn/GeSn DHS.

Our theoretical considerations indicate that large offsets in type I SiGeSn/GeSn MQW can be obtained. Similarly as for calculations of GeSn/Ge MQWs the bandgaps, deformation

#254548 Received 24 Nov 2015; revised 29 Dec 2015; accepted 30 Dec 2015; published 15 Jan 2016

potentials, and effective masses were taken as listed in [28], average valence band offsets of constituents from [22], the bandgaps bowing for GeSn was taken from [31], and for SiGe and SiSn from [32]. Luttinger parameters for SiGeSn were calculated by first using quadratic interpolation of data from [24], (see also [1]-SI) for the (GeSn) part of the ternary alloy, and then linearly interpolation for Si(GeSn). Results in Fig. 4(a) show the evolution of energy offsets in $Si_xGe_{0.9-x}Sn_{0.1}/Ge_{0.88}Sn_{0.12}$ heterostructures depending on the Si content in the SiGeSn buffer. For the active region of GeSn a residual compressive strain of −0.47% is considered including the assumption of coherently grown SiGeSn claddings. The incorporation of a high amount of Si enables the creation of heterostructures with a potential of high confinement due to band offsets of up to 0.26 eV (for 14 at. % Si).

According to the goal of achieving efficient light emitters, we present in Fig. 4(b) the electronic band structure of a {SiGeSn/GeSn} MQW with {20 nm $Si_{0.08}Ge_{0.81}Sn_{0.11}$ barriers/ 10 nm $Ge_{0.88}Sn_{0.12}$ wells}. The band offset for Γ, L as well as HH and LH bands are given in Table 1. Furthermore, an optimized growth strategy allows to improve the band offset at the lower interface by introducing a $Si_{0.15}Ge_{0.81}Sn_{0.04}$ layer as a large bandgap barrier. SIMS spectra of such epitaxially grown heterostructure including p- and n-type doping is shown in Fig. 4(c) on a TEM cross-section image. The different elements are clearly resolved inside the layer stack. The dislocation network is mainly located at the interface between Ge-VS and first SiGeSn layer, providing a good layer quality to the main part of the heterostructure (including the active GeSn layer). Applying such growth techniques in the future, additional, more complex SiGeSn/GeSn structures will be considered for the fabrication of efficient LEDs.

Table 1: Material and band structure parameters for the investigated (Si)Ge(Sn)/GeSn DHS and MQW. All values of band offsets come from calculations.

Structure	Sn Content (%)	GeSn Strain (%)	ΔE_Γ (meV)	ΔE_L (meV)	ΔE_{LH} (meV)	ΔE_{HH} (meV)	GeSn DBG*	Type I at Γ point	Type I at Γ and L
GeSn homojunction (exp)	8	–0.34	0	0	0	0		No	No
GeSn/Ge MQW (exp)	8	–0.71	27	–17	31	150	o	Yes	No
GeSn/Ge DHS (th)	12.5	–0.7	34	–32	18	233	Yes	Yes	No
GeSn/Ge DHS (th)	12.5	–0.47	33	–31	3	233	Yes	Yes	No
GeSn/SiGeSn** DHS (exp)	12	–0.47	475 / 171	81 / 24	141/47	196 / 84	Yes	Yes	Yes
GeSn/SiGeSn*** MQW (th)	12.5	–0.47	171	24	47	84	Yes	Yes	Yes

*DBG- fundamental direct bandgap

**$Si_{0.15}Ge_{0.81}Sn_{0.04}/Ge_{0.88}Sn_{0.12}/Si_{0.08}Ge_{0.81}Sn_{0.11}$

***$Si_{0.08}Ge_{0.81}Sn_{0.11}$

5. Conclusion

We have presented the growth and electro-optical characterization of both *p-i-n* GeSn homojunction and {GeSn/Ge} MQW LEDs with Sn content of 8 at. %. Small injection current density thresholds (about 30-50 A/cm^2) are needed in order to induce light emission in both types of LEDs, despite the still indirect bandgap of the alloys. Both experimental and theoretical investigations indicate that Ge can serve as a barrier material for electron confinement only for low Sn content, still indirect bandgap GeSn alloys. In our structures,

#254548 Received 24 Nov 2015; revised 29 Dec 2015; accepted 30 Dec 2015; published 15 Jan 2016

partially relaxed layers with Sn contents between 7 and 8 at. %, the Ge layers act as well and GeSn as barrier for L electrons. For fundamental direct bandgap GeSn alloys (with large Sn contents well above 8 at. % in buffer and well), Ge layers are rather weak barriers due to the induced tensile strain. Therefore an optimum Ge/GeSn configuration offers only band offsets of around 40 meV at L and Γ-point. However, calculations indicate that SiGeSn alloys, in the experimentally accessible Si and Sn concentrations range, could successfully be employed as barriers for direct bandgap GeSn wells with band offsets much larger than 25 meV. The growth of such a SiGeSn/GeSn DHS with corresponding band structure calculations was demonstrated, proving suitability and feasibility. Therefore a configuration of this kind is most promising for future light emitting devices.

Acknowledgments

This research received funding for CVD growth investigations from Federal Ministry of Education and Research (BMBF) under project UltraLowPow (16ES0060 K). The authors also acknowledge funding from The Royal Society International Exchanges grant IE131593. We thank Steffi Lenk for their assistance with TEM measurements.

#254548 Received 24 Nov 2015; revised 29 Dec 2015; accepted 30 Dec 2015; published 15 Jan 2016